nature photonics

ARTICLES

https://doi.org/10.1038/s41566-022-01028-5

Observation of toroidal pulses of light

Apostolos Zdagkas[1], Cormac McDonnell[2], Junhong Deng[3,4], Yijie Shen[1], Guixin Li[3,4], Tal Ellenbogen[2], Nikitas Papasimakis[1]✉ and Nikolay I. Zheludev[1,5]

Transverse electromagnetic waves are important carriers of information and energy. In 1996, Hellwarth and Nouchi theoretically identified a radically different, non-transverse type of electromagnetic pulse with a toroidal topology. These pulses, which are propagating counterparts of localized toroidal dipole excitations in matter, exhibit unique electromagnetic wave properties and, so far, have never been experimentally realized and observed. Here we report the generation of such toroidal light pulses in the optical and terahertz regions by the use of tailored nanostructured meta-surfaces. This achievement paves the way for experimental studies of energy and information transfer with toroidal light pulses, their space–time coupling and their light–matter interactions involving anapoles, localized space–time coupled excitations, skyrmions and toroidal qubits, which are of growing interest for the fundamental science of light and applications.

The emerging research field of toroidal electrodynamics has been attracting growing interest since experimental observations of the oscillating toroidal dipole in 2010[1] and dynamic electromagnetic anapoles in 2013[2]. This has been stimulated by the intriguing electromagnetic properties of toroidal dipoles, such as odd space and time symmetry, complementarity to the electric and magnetic dipoles[3], and predictions of their involvement in non-reciprocal electromagnetic interactions[4]. Dynamic toroidal dipoles have been observed in artificial materials and nanostructures in the microwave regime and across the optical part of the spectrum[5–9]. They are now recognized as indispensable contributors to the linear and nonlinear optical properties of matter[10,11]. As such, new types of spectroscopy, including atomic spectroscopy[12], that are selective to the optical transitions enabled by toroidal dipoles are being developed based on solvatochromism[13] and standing-wave illumination[14]. Furthermore, dynamic anapoles, co-located non-radiating configurations of oscillating electric and toroidal dipoles[2], are attracting interest as a vehicle for high-quality resonant devices[15–17], quantum qubits[18] and even reservoirs of dark energy[19]. Although anapole modes do not radiate electromagnetic fields, they arguably emit vector potential waves that are not removable by gauge transforms and may lead to new types of the Aharonov–Bohm phenomenon[20,21].

Since 1996 it has been understood from the work of Hellwarth and Nouchi that oscillating toroidal excitations can also exist in the form of bursts of electromagnetic energy propagating in free space at the speed of light[22]. Although such toroidal light pulses (TLPs) travel at the speed of light, they are radically different from conventional plane electromagnetic waves on several counts:

(1) TLPs possess non-transverse electromagnetic field components. Indeed, the conventional plane electromagnetic waves that we have known since the early days of Heinrich Rudolf Hertz and that are used in modern free-space telecommunication technologies are transverse electromagnetic waves, in which the electric and magnetic fields oscillate in a direction perpendicular to the direction of propagation. TLPs are not transverse, but instead present a toroidal topology, with the magnetic field tracing the body of a doughnut-like shape while the electric field traces its surface, exhibiting electric-field components that are oriented along the direction of pulse propagation (Fig. 1a). A complementary form of TLPs with a component of magnetic field oscillating along the direction of propagation can be obtained by exchanging the electric and magnetic fields[22]. These two forms are known as transverse magnetic (TM) and transverse electric (TE) TLPs, respectively.

(2) TLPs are space–time non-separable. Plane waves belong to a family of solutions to Maxwell's equations that can be presented as a product of time- and space-dependent complex exponential functions and that include, for example, Gaussian, Bessel and Airy waves and pulses. However, it has been known since the early 1980s that Maxwellian electrodynamics admit solutions where the space and time dependences are non-separable; that is, they cannot be presented as a product of the time-only and space-only dependent terms[23–27]. TLPs belong to this category: they are exact solutions to Maxwell's equations, but they are of a non-separable nature[22] (Supplementary Section 1 describes analytical formulae describing such pulses). The space–time non-separability of the TLPs manifests in the space-spectrum domain as a position-dependent frequency content across the transverse plane. Here, the lower-frequency components dominate at the periphery of the toroidal pulse, while higher frequencies prevail at its central area (Fig. 1a,b).

(3) TLPs are single-cycle pulses. Elementary TLPs exist as short localized, single or 1½ cycle bursts of radiation with a broad spectrum and finite total energy. Upon propagation, the TLPs focus and defocus and experience reshaping due to a propagation-dependent Gouy phase term[28]: TLPs of the first type evolve from 1½ cycles away from the focus to single-cycle pulses at focus, then back to the 1½-cycle pulses (Fig. 1a). Similarly, TLPs of the second type are single cycle away from focus and 1½ cycle at focus. The Hellwarth and Nouchi TLPs are characterized by two parameters, q_1 and q_2, which correspond to the effective wavelength and the length of the focal region, respectively[22] (Supplementary Section 1).

[1]Optoelectronics Research Centre and Centre for Photonic Metamaterials, University of Southampton, Southampton, UK. [2]Department of Physical Electronics, School of Electrical Engineering, Tel-Aviv University, Tel Aviv, Israel. [3]Department of Materials Science and Engineering, Southern University of Science and Technology, Shenzhen, China. [4]Shenzhen Institute for Quantum Science and Engineering, Southern University of Science and Technology, Shenzhen, China. [5]Centre for Disruptive Photonic Technologies, School of Physical and Mathematical Sciences and the Photonics Institute, Nanyang Technological University, Singapore, Singapore. ✉e-mail: n.papasimakis@soton.ac.uk

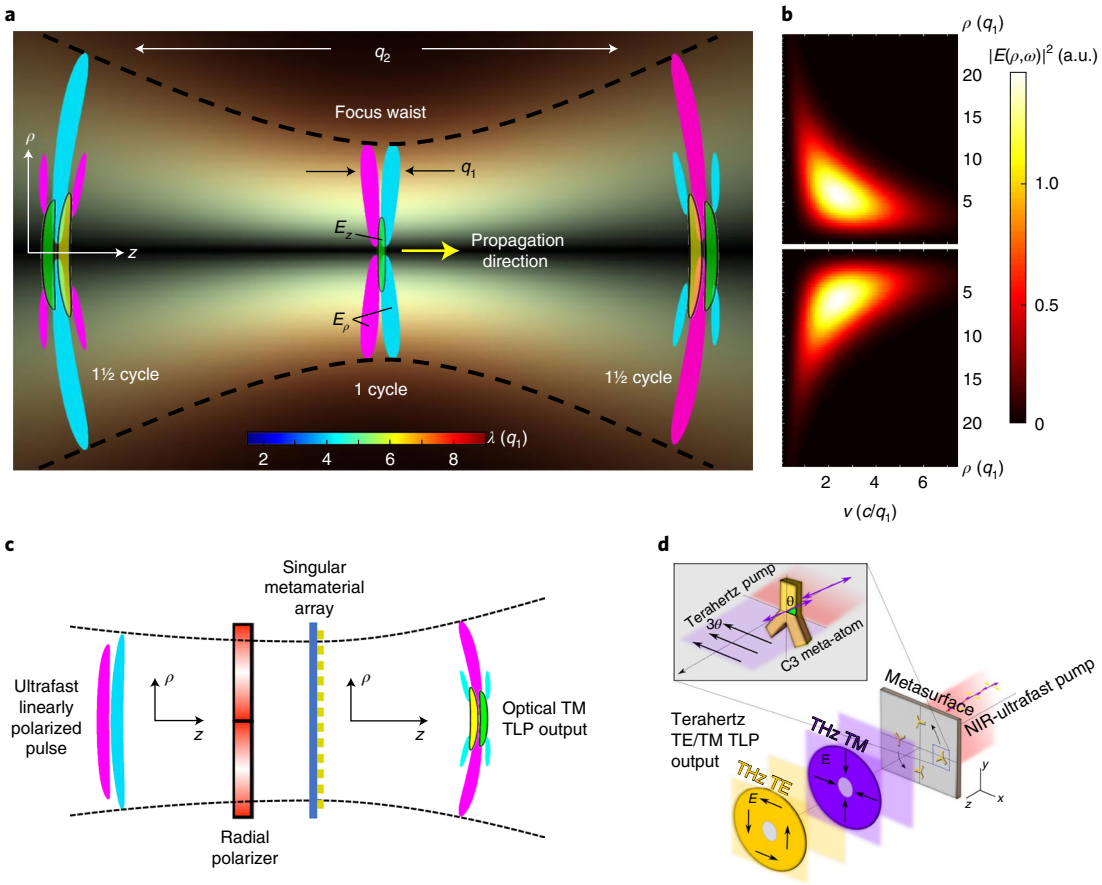

Fig. 1 | Characteristics of TLPs and blueprint for their generation. a,**b**, Spatiotemporal and spatio-spectral structure of the TM TLP. In **a**, the propagation of the TLP is shown. Frequency and intensity are represented by colour and brightness, respectively. Red and blue coloured regions indicate prevalent long- and short-wavelength components, respectively, and white regions represent broadband spectral content of the pulse (see Supplementary Section 4 for details). The dashed lines mark the trajectory traced by the waist of the pulse. Cyan and magenta (green and yellow) lobes represent half-cycles of the transverse, E_ρ (longitudinal, E_z) component of the electric field of the pulse with opposite signs. At focus, the electric field of the TM TLP consists of two toroidal lobes of transverse fields connected by a single lobe of strong longitudinal field. The propagation of the pulse is controlled by the parameters q_1 and q_2, which play the role of effective wavelength and Rayleigh range, respectively. In **b**, space–time coupling in the TLP is shown manifested in the distribution of frequency components along the radial direction ρ: the higher-frequency components are closer to the pulse centre and lower-frequency components are at the periphery of the pulse ($|\rho| \gg q_1$). The presented spectra correspond to a TLP at focus. Frequency is in units of c/q_1. **c**, Schematic of the generation of TM TLPs in the optical part of the spectrum. A linearly polarized ultrafast pulse is converted to a radially polarized pulse by a segmented waveplate that acts as a broadband polarization converter. The TLPs are then launched by a singular specially tailored plasmonic meta-surface excited with the radially polarized pulse. Cyan and magenta lobes correspond to half-cycles of the electric field of the input pulse and output pulses. **d**, Generation of terahertz (THz) TM and TE TLPs using plasmonic meta-surfaces. The meta-surface is illuminated with near-infrared ultrashort pulses (~50 fs). The C3 meta-atoms (inset) then radiate electromagnetic waves in the terahertz spectral region through an optical rectification process. The spatial arrangement of the meta-atoms is designed to generate the TLPs.

(4) TLPs exhibit a space–time toroidal topology. The unique space–time toroidal structure of TLPs contains multiple singularities and areas of energy backflow (zones where electromagnetic energy propagates opposite to the energy mainstream of the pulse) that are identifiable at the low-intensity areas of the pulse[29].

Results and discussion

Until now, the Hellwarth and Nouchi TLPs—the propagating counterparts of localized toroidal modes[1] and exact solutions of Maxwell's equation—have not been observed, and the generation and characterization of such pulses presents a formidable challenge due to their complex spatio-spectral structure, short duration and topology. Beyond being a fundamental manifestation of a stable electromagnetic free-space structure with toroidal topology, the Hellwarth and Nouchi pulses are also an acknowledged example of non-separable waves[27,30] and are attracting growing attention in electromagnetics and acoustics (refs. [31–35] and references therein). Such non-separable pulses have been studied theoretically[36,37] and can emerge through filamentation[38,39] with little or no control over the space–time coupling. In this Article we report two complementary approaches to the generation of TLPs, in the optical and terahertz spectral ranges, respectively. Whereas the generated optical TLPs are a few cycles long (limited by the bandwidth of the laser source), in the terahertz part of the spectrum, we report single-cycle TLPs. Both approaches are based on using arrays of nanostructured emitters of toroidal topology that are driven by conventional laser light pulses (Fig. 1c,d). In the optical part of the spectrum, we use a linear meta-surface designed to scatter conventional laser pulses into few-cycle optical TLPs (Fig. 1c), whereas in the terahertz range we employ a nonlinear meta-surface that rectifies the envelopes of the incident laser pulses and re-radiates them as single-cycle terahertz TLPs (Fig. 1d).

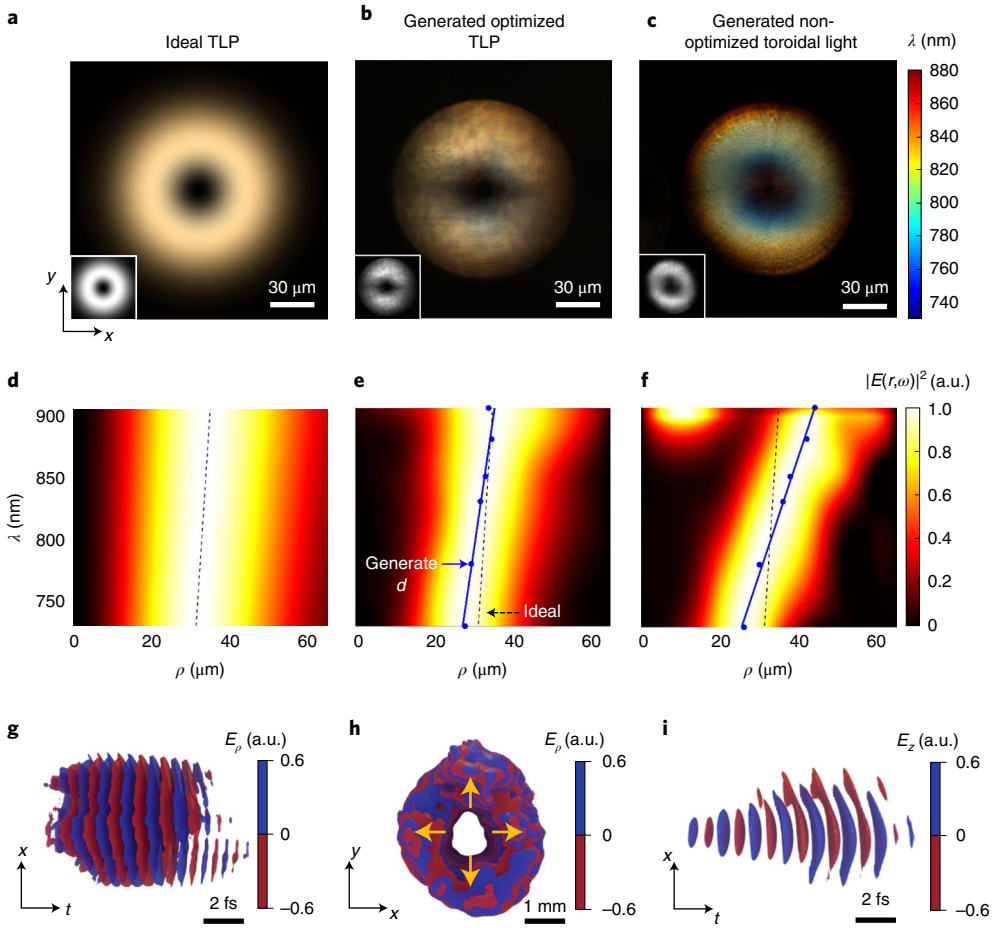

Fig. 2 | The spatio-spectral and spatiotemporal structure of generated optical TLPs. a–c, A comparison of hyperspectral images of the transverse profiles of ideal TLPs computed analytically (**a**) and the experimental profiles of experimentally generated TLPs (**b**). The profile in **c** is of a pulse generated by a meta-surface with excessively large space-spectrum coupling. Insets to **a–c** present the energy density profiles of the pulses shown in the corresponding panels. **d–f**, Radial distribution of the spectral density for the pulses presented in **a–c**, respectively. The dashed and solid lines track the energy density maxima of the ideal TLP and experimentally generated pulses, respectively. **g–i**, Details of the structure of the optimized pulse retrieved by interferometry. The interference is performed on the expanded and collimated pulse, in contrast to **a–f**, which correspond to the pulse at focus. Side and front views of the transverse electric field component are shown in **g** and **h**, and a side view of the longitudinal component is shown in **i** (Supplementary Video 1 and Supplementary Section 5). Red and blue colours represent regions of electric field with opposite phases. We note that the generated TLPs are a few cycles long as a result of bandwidth limitations of the laser system used in the experiments.

Optical TLPs. The generation scheme for optical TLPs comprises a linear-to-radial polarization converter and a nanostructured meta-surface (Fig. 1c) that are driven by few-cycle (<10 fs at full-width at half-maximum (FWHM)) linearly polarized laser pulses with a central wavelength of ~800 nm and bandwidth of ~200 nm. The meta-surface consists of concentric gold rings. The width of the rings and thus their resonant plasmonic properties vary with the ring radius in such a way that re-radiated light accrues phases and amplitudes according to the spatiotemporal coupling of the TLPs (Supplementary Section 2)[40]. The varying pitch of the meta-surface, as well as all the local radial features, remain smaller than the shortest wavelength of the input pulse for all radii. As such, the meta-surface supports scattering into the tailored zeroth-order TLP with negligible higher-order diffraction.

In our experiments we targeted the generation of ideal TLPs that can be fully defined by the effective wavelength, q_1, and Rayleigh range, q_2. The effective wavelength is determined so that the spectral peak of the target pulse coincides with the centre wavelength of our laser system (~800 nm). The structural dimensions of the meta-surface and divergence of the pump beam control the Rayleigh range. The plasmonic meta-surface is designed with the transmission resonance wavelength varying along the radial direction so as to achieve $q_1 = 192$ nm and $q_2 = 75{,}000 q_1$. To emphasize the importance of the design, a second meta-surface arrangement was used to create pulses of toroidal symmetry, but with excessively large space-spectrum coupling that is incompatible with the spatio-spectral structure of ideal TLPs (Supplementary Section 2).

The spatiotemporal and spatio-spectral structures of the generated optical TLPs were characterized by hyperspectral imaging of their transverse profiles (as constructed from multiple images at different wavelengths; Supplementary Section 4 and Fig. 2a–f) and by spatially resolved Fourier-transform interferometry[41,42]. The latter approach is based on interference of the generated TLP with a known reference linearly polarized pulse, allowing retrieval of the spectral amplitude and phase for all polarization components of the electric field at any point of the TLP (Supplementary Section 3 and Fig. 2g–i).

The results of the spectral and interferometric measurements confirm the toroidal topology of the generated pulses and compliance with the characteristics of the ideal TLP (Fig. 1a). In the

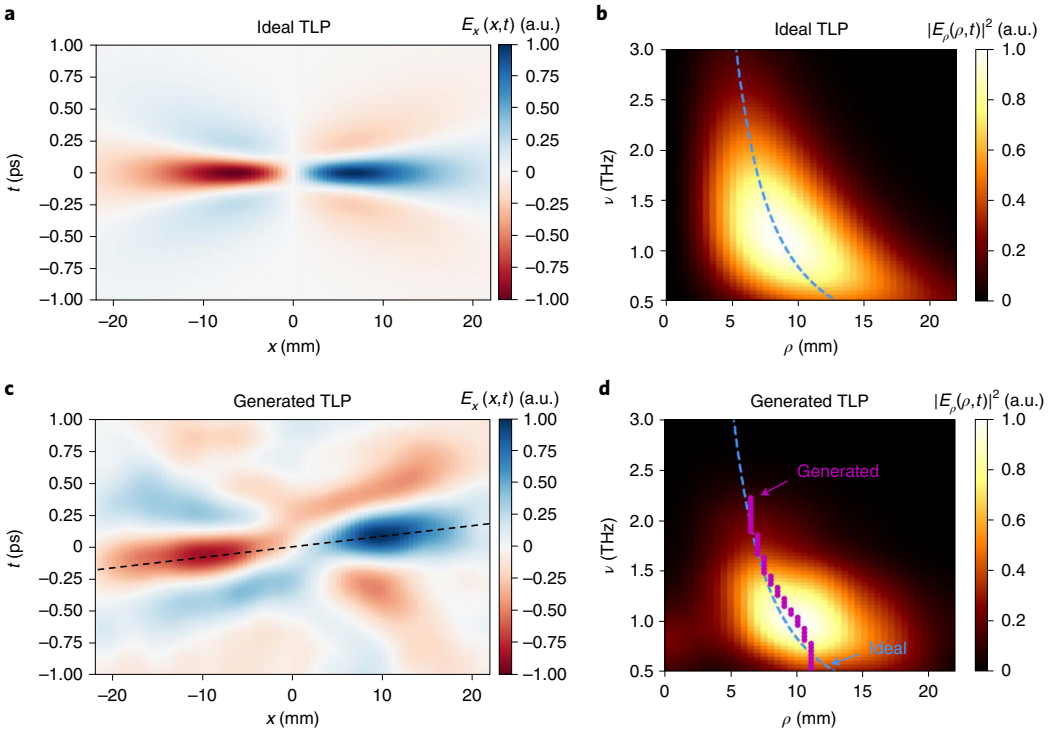

Fig. 3 | The spatiotemporal and spatio-spectral structure of generated terahertz TLPs. a–d, Spatiotemporal maps (**a**,**c**) and spatial variations of the spectrum (**b**,**d**) for an ideal (**a**,**b**) and generated (**c**,**d**) terahertz TM TLP. Blue dashed lines and purple markers in **b** and **d** track the energy density maxima of the ideal and experimentally generated pulses, respectively. The black dashed line in **c** serves as a guide to the eye, indicating a small tilt in the experimentally generated pulse. The parameters of the ideal TLP are $q_1 = 63\,\mu m$ and $q_2 = 56{,}000 q_1$.

generated pulses, the lower-frequency components are dominant at the periphery of the profile, while higher frequencies prevail in its central part (Fig. 2b,e). Here, the main qualitative measure of the correct space-spectrum non-separability is the gradual wavelength-dependent shift of the radial position of the spectral components of the experimentally generated pulses, which closely matches that of the ideal TLP (Fig. 2a,d). In comparison, the hyperspectral profile of the pulses generated by the meta-surface with excessive space-spectrum coupling (Fig. 2c,f) deviates substantially from that of the ideal TLP. The vectorial spatial interferometry used in our experiments is capable of reconstructing all the components of the electric and magnetic fields. Figure 2g–i shows isosurfaces of the electric field of the generated TLP at a level of 60% of its maximum. Red and blue colours correspond to the two half-cycles of the pulse. As expected, the electric field presents vanishing transverse components at the centre of the pulse (Fig. 2h) but exhibits substantial longitudinal components (Fig. 2i).

To quantify the similarity of the targeted pulses to the ideal TLPs, we used an intensity-distribution state tomography approach analysing a discrete set of spatial and spectral states of the pulses[27]. This method returns a fidelity measure, $0 < F < 1$, where $F = 1$ indicates perfect similarity of the pulses, and small fidelity values correspond to a lack of similarity (details are provided in Supplementary Section 10). The pulses generated with the optimized meta-surface (Fig. 2b,e) exhibited a high fidelity of $F = 0.79$, and pulses generated by the meta-surface with excessively large spectral shift (Fig. 2c,f) delivered $F = 0.1$.

The spatiotemporal and spatio-spectral characterizations of the generated optical pulses thus reveal the main features of ideal TLPs: (1) the presence of a non-TE field component (Fig. 2i); (2) the non-separable spatio-spectral structure of the generated pulses, as quantified by a high fidelity value; (3) few-cycle pulse duration (owing to the limited bandwidth of the laser system, the generated pulses have a duration of a few cycles and thus are not elementary single-cycle TLPs; the generation of single-cycle TLPs will be described in the terahertz section of this paper); (4) owing to their space–time non-separability, TLPs propagate with no distortion of their spatio-spectral profiles (Supplementary Section 11); (5) the generated optical pulses exhibit a profound toroidal topology. Observation of topological features such as singularities and energy backflow was not targeted in the current work as these features occur at the areas of lower energy that are inaccessible to vectorial spatial interferometry. Finally, we have confirmed experimentally that the generated TLPs do not carry orbital angular momentum (OAM), in accordance with theoretical predictions[22] (Supplementary Section 12).

Terahertz TLPs. We generated single-cycle TLPs in the terahertz part of the spectrum through optical rectification of femtosecond near-infrared pulses (~50 fs with a centre wavelength of ~1,500 nm) on a Pancharatnam–Berry phase meta-surface[43–46]. We used a plasmonic meta-surface consisting of a cylindrically symmetric array of gold meta-atoms of three-fold (C^3) rotational symmetry (Fig. 1d and Supplementary Section 6). Orientation of the principal axis of the meta-atoms at an angle θ with respect to the linear polarization direction of the pump near-infrared pulse results in the generation of single-cycle terahertz waves, linearly polarized at an angle of 3θ (ref. [46]), as shown schematically in Fig. 1d. Arranging the meta-atoms on the circularly symmetric meta-surface with their principal axis rotating 120° around the circumference can be used for the generation of TM-polarized or TE-polarized TLPs depending on the incident polarization of the pump pulse (0° for TE and 45° for TM). All other pump linear polarizations will result in a mixed TE and TM beam of varying degrees depending on the exact angle. For example, a pump pulse polarization angle of 22.5° results in an exact hybrid TE/TM polarization, as illustrated in Supplementary Fig. 9. The generated TE and TM pulses are characterized in the spatial and time domain,

with raster-scanning in two spatial dimensions (Supplementary Section 7). The generated terahertz TM pulse for a pumping polarization angle of 45° exhibits a sub two-cycle duration similar to the 1½-cycle ideal TLP (Fig. 3). Both the ideal TLP and the generated pulse exhibit reverse signs of the E_x field on opposite sides of the $x=0$ plane (red and blue coloured regions in Fig. 3a,c) and take minimum values at the centre of the pulse (for $x=0$). The same spatial characteristics are measured for the E_y field on opposite sides of the $y=0$ plane, indicating polarization along the radial direction (Supplementary Section 8). The space–time non-separable natures of the ideal and generated TLPs are presented in Fig. 3b,d, respectively, in the form of the spatial profile of the corresponding frequency spectra. The space-spectral non-separability here manifests in the shift of the energy density maxima position from short to longer radii with decreasing frequency: the corresponding traces of the energy density maxima follow closely spaced trajectories in the spatio-spectral plane (frequency–radius). The corresponding value of space-spectral non-separability fidelity is $F=0.80$ (Supplementary Section 10). Therefore, the generated terahertz pulses exhibit the main features of the ideal TLPs: (1) an electric field with radial and longitudinal components (Fig. 3c); (2) space–time non-separability with high fidelity (Fig. 3d); (3) pulse duration close to the single- to 1½-cycle ideal TLP (Fig. 3a,c); (4) toroidal topology. The corresponding TE mode for a pumping polarization angle of 0° is shown in Supplementary Fig. 8.

Conclusions

We have demonstrated the generation and detection of TLPs in the optical and terahertz parts of the spectrum and mapped their temporal and spectral characteristics and space–time structures. Such light pulses are fundamental space–time non-separable exact solutions of Maxwell's equations and prime candidates for the investigation of toroidal light–matter interactions involving the excitation of toroidal and anapole modes in matter[47,48]. The few-cycle nature of TLPs will be of particular interest for the study of transient and nonlinear aspects of toroidal and anapole excitations, and their space–time non-separable structure is expected to lead to non-trivial phenomena. Moreover, TLPs have recently been found to be the foundational members of the family of super toroidal light pulses, which have exciting optical properties and skyrmionic field structure[49]. Finally, their unique propagation dynamics could lead to novel spectroscopic and manufacturing-with-light applications, and interesting information and energy transfer schemes.

Online content

Any methods, additional references, Nature Research reporting summaries, source data, extended data, supplementary information, acknowledgements, peer review information; details of author contributions and competing interests; and statements of data and code availability are available at https://doi.org/10.1038/s41566-022-01028-5.

Received: 17 April 2021; Accepted: 25 May 2022;
Published online: 1 July 2022

References

1. Kaelberer, T., Fedotov, V. A., Papasimakis, N., Tsai, D. P. & Zheludev, N. I. Toroidal dipole response in a metamaterial. *Science* **10**, 1510–1512 (2010).
2. Fedotov, V. A., Rogacheva, A. V., Savinov, V., Tsai, D. P. & Zheludev, N. I. Resonant transparency and non-trivial non-radiating excitations in toroidal metamateirals. *Sci Rep.* **3**, 2967 (2013).
3. Dubovik, V. M. & Tugushev, V. V. Toroid moments in electrodynamics and solid-state physics. *Phys. Rep.* **187**, 145–202 (1990).
4. Afanasiev, G. N. Simplest sources of electromagnetic fields as a tool for testing the reciprocity-like theorems. *J. Phys. D* **34**, 539 (2001).
5. Ding, C. et al. Stable terahertz toroidal dipolar resonance in a planar metamaterial. *Phys. Status Solidi* **252**, 1388–1393 (2015).
6. Gupta, M. et al. Sharp toroidal resonances in planar terahertz metasurfaces. *Adv. Mater.* **28**, 8206–8211 (2016).
7. Ögüt, B., Talebi, N., Vogelgesang, R., Sigle, W. & van Aken, P. A. Toroidal plasmonic eigenmodes in oligomer nanocavities for the visible. *Nano Lett.* **12**, 5239–5244 (2012).
8. Dong, Z. G. et al. Optical toroidal dipolar response by an asymmetric double-bar metamaterial. *Appl. Phys. Lett.* **101**, 144105 (2012).
9. Wu, P. C. et al. Three-dimensional metamaterials: from split ring resonator to toroidal metamolecule. *Proc. SPIE* **9163**, 91630M (2014).
10. Papasimakis, N., Fedotov, V. A., Savinov, V., Raybould, T. A. & Zheludev, N. I. Electromagnetic toroidal excitations in matter and free space. *Nat. Mater.* **15**, 263–271 (2016).
11. Smirnova, D. & Kivshar, Y. S. Multipolar nonlinear nanophotonics. *Optica* **3**, 1241–1255 (2016).
12. Kuprov, I., Wilkowski, D. & Zheludev, N. I. Toroidal optical transitions in hydrogen-like atoms. Preprint at https://arxiv.org/abs/2205.01412 (2022).
13. Savinov, V., Papasimakis, N., Tsai, D. P. & Zheludev, N. I. Optical anapoles. *Commun. Phys.* **2**, 69 (2019).
14. Tseng, M. L. et al. Coherent selection of invisible high-order electromagnetic excitations. *Sci. Rep.* **7**, 44488 (2017).
15. Miroshnichenko, A. E. et al. Nonradiating anapole modes in dielectric nanoparticles. *Nat. Commun.* **6**, 8069 (2015).
16. Yang, Y. Q., Zenin, V. A. & Bozhevolnyi, S. I. Anapole-assisted strong field enhancement in individual all-dielectric nanostructures. *ACS Photon.* **5**, 1960–1966 (2018).
17. Xu, L. Boosting third-harmonic generation by a mirror-enhanced anapole resonator. *Light Sci. Appl.* **7**, 44 (2018).
18. Zagoskin, A. M., Chipouline, A., Il'ichev, E., Johansson, J. R. & Nori, F. Toroidal qubits: naturally-decoupled quiet artificial atoms. *Sci. Rep.* **5**, 16934 (2015).
19. Gao, Y., Ho, C. M. & Scherrer, R. J. Anapole dark matter at the LHC. *Phys. Rev. D* **89**, 045006 (2014).
20. Marengo, E. A. & Ziolkowski, R. W. Nonradiating sources, the Aharonov-Bohm effect, and the question of measurability of electromagnetic potentials. *Radio Sci.* **37**, 19-1–19-10 (2002).
21. Nemkov, N. A., Baharin, A. A. & Fedotov, V. A. Nonradiating sources, dynamic anapole and Aharonov –Bohm effect. *Phys. Rev. B* **95**, 165134 (2017).
22. Hellwarth, R. W. & Nouchi, P. Focused one-cycle electromagnetic pulses. *Phys. Rev. E* **54**, 889–895 (1996).
23. Brittingham, J. N. Focus waves modes in homogeneous Maxwell equations—transverse electric mode. *J. Appl. Phys.* **54**, 1179–1189 (1983).
24. Ziolkowski, R. W. Exact-solutions of the wave-equation with complex source locations. *J. Math. Phys.* **26**, 861–863 (1985).
25. Ziolkowski, R. W. Localized transmission of electromagnetic energy. *Phys. Rev. A* **39**, 2005–2033 (1989).
26. Zdagkas, A., Papasimakis, N., Savinov, V. & Zheludev, N. I. Space-time non-separable pulses: constructing isodiffracting donut pulses from plane waves and single-cycle pulses. *Phys. Rev. A* **102**, 063512 (2020).
27. Shen, Y., Zdagkas, A., Papasimakis, N. & Zheludev, N. I. Measures of space-time non-separability of electromagnetic pulses. *Phys. Rev. Res.* **3**, 013236 (2021).
28. Feng, S., Winful, H. G. & Hellwarth, R. W. Gouy shift and temporal reshaping of focused single-cycle electromagnetic pulses. *Opt. Lett.* **23**, 385–387 (1998).
29. Zdagkas, A., Papasimakis, N., Savinov, V., Dennis, M. R. & Zheludev, N. I. Singularities in the flying electromagnetic doughnuts. *Nanophotonics* **8**, 1379 (2019).
30. Shen, Y. & Rosales-Guzmán, C. Nonseparable states of light: from quantum to classical. *Laser Photon. Rev.* **2022**, 2100533 (2022).
31. Reivelt, K. & Saari, P. Localized wave solutions of the scalar homogeneous wave equation and their optical implementation. Preprint at https://arxiv.org/abs/physics/0309079 (2020).
32. Saari, P. & Reivelt, K. Evidence of X-shaped propagation-invariant localized light waves. *Phys. Rev. Lett.* **79**, 4135–4138 (1997).
33. Hernández-Figueroa, H. E., Recami, E. & Zamboni-Rached, M. *Non-Diffracting Waves* (Wiley, 2014).
34. Bhaduri, B., Yessenov, M. & Abouraddy, A. F. Anomalous refraction of optical spacetime wave packets. *Nat. Photon.* **14**, 416–421 (2020).
35. Kondakci, H. E. & Abouraddy, A. F. Diffraction-free space–time light sheets. *Nat. Photon.* **11**, 733–740 (2017).
36. Porras, M. A., Borghi, R. & Santarsiero, M. Few-optical-cycle Bessel-Gauss pulsed beams in free space. *Phys. Rev. E* **62**, 5729–5737 (2000).
37. Porras, M. A., Valiulis, G. & Di Trapani, P. Unified description of Bessel X waves with cone dispersion and tilted pulses. *Phys. Rev. E* **68**, 016613 (2003).
38. Couairon, A. & Mysyrowicz, A. Femtosecond filamentation in transparent media. *Phys. Rep.* **441**, 47–189 (2007).
39. Jhajj, N. et al. Spatiotemporal optical vortices. *Phys. Rev. X* **6**, 031037 (2016).

40. Papasimakis, N. et al. Pulse generation scheme for flying electromagnetic doughnuts. *Phys. Rev. B* **97**, 201409 (2018).
41. Zdagkas, A., Nalla, V., Papasimakis, N. & Zheludev, N. I. Spatiotemporal characterization of ultrashort cylindrical vector pulses. *APL Photon.* **6**, 116103 (2021).
42. Pariente, G., Gallet, V., Borot, A., Gobert, O. & Quere, F. Space–time characterization of ultra-intense femtosecond laser beams. *Nat. Photon.* **10**, 547–553 (2016).
43. Luo, L. et al. Broadband terahertz generation from metamaterials. *Nat. Commun.* **5**, 3055 (2014).
44. Polyushkin, D. K., Hendry, E., Stone, E. K. & Barnes, W. L. THz generation from plasmonic nanoparticle arrays. *Nano Lett.* **11**, 4718–4724 (2011).
45. Keren-Zur, S., Tal, M., Fleischer, S., Mittleman, D. M. & Ellenbogen, T. Generation of spatiotemporally tailored terahertz wavepackets by nonlinear metasurfaces. *Nat. Commun.* **10**, 1778 (2019).
46. McDonnell, C., Deng, J., Sideris, S., Ellenbogen, T. & Li, G. Functional THz emitters based on Pancharatnam–Berry phase nonlinear metasurfaces. *Nat. Commun.* **12**, 30 (2021).
47. Raybould, T., Fedotov, V. A., Papasimakis, N., Youngs, I. & Zheludev, N. I. Exciting dynamic anapoles with electromagnetic doughnut pulses. *Appl. Phys. Lett.* **111**, 081104 (2017).
48. Raybould, T., Fedotov, V. A., Papasimakis, N., Youngs, I. & Zheludev, N. I. Focused electromagnetic doughnut pulses and their interaction with interfaces and nanostructures. *Opt. Exp.* **24**, 3150–3161 (2016).
49. Shen, Y., Hou, Y., Papasimakis, N. & Zheludev, N. I. Supertoroidal light pulses as electromagnetic skyrmions propagating in free space. *Nat. Commun.* **12**, 5891 (2021).

Methods

Sample fabrication. The optical meta-surface consists of concentric plasmonic rings fabricated by focused-ion beam milling of a 50-nm-thick gold film supported by a 100-nm-thick dielectric Si_3N_4 membrane. The width of the plasmonic rings varies radially, with narrower rings at the centre of the meta-surface and broader rings at the periphery, and with the gap between adjacent rings remaining constant at 100 nm (Supplementary Section 2).

The terahertz meta-surface was fabricated by an electron-beam lithography process (Supplementary Section 6). In the first step, a thin positive electron resist layer (2.5% poly(methyl methacrylate), Allresist) was prepared on an indium tin oxide thin film on a glass substrate using spin-coating, which was followed by baking at 180 °C for 3 min. The designed patterns for the meta-atoms were then transferred to the prepared photoresist layer by electron-beam lithography. Finally, a 30-nm-thick gold layer was deposited onto the photoresist layer using an electron-beam evaporator, which formed the plasmonic meta-surface after a lift-off process.

Pulse characterization. The vectorial spatiotemporal shape of the optical pulse was measured by spatially resolved Fourier-transform spectroscopy[41]. First, a linearly polarized pulse was fully characterized with a self-referenced method[42]. A Michelson interferometer was implemented such that the linearly polarized pulse was interfered with an expanded replica of itself and the energy density profile was captured on a camera sensor while a translation stage shifted the relative position between the two pulses. An iterative algorithm was then applied to the data to retrieve the spatially dependent spectral phase. The pulse was compressed into its Fourier-limited duration by a liquid-crystal-based spatial light modulator (Biophotonics MIIPS Box640)[50].

The characterized linearly polarized pulse was interfered with the unknown vector polarized pulse in a Mach–Zehnder interferometer (Supplementary Section 3). The spectral phase of the two orthogonal polarizations of the vector polarized pulse was characterized separately for each polarization. The longitudinal field was then calculated from Gauss's law in free space and the measured transverse electromagnetic fields (Supplementary Section 5), and the magnetic field was calculated from Faraday's law and the electric field. The spatio-spectral profile was characterized at the plane of the meta-surface with a set of narrowband filters, 10-nm FWHM and a camera sensor (Supplementary Section 4).

The temporal shape of the terahertz pulse was characterized with a time-domain spectroscopy set-up based on the electro-optic effect (ZnTe crystal) with a 35-fs probe pulse centred at 800 nm, a Wollaston prism and a balanced photodiode (Supplementary Section 7). The overlap between the terahertz and the probe pulse on the ZnTe crystal was shifted by adding a delay line on the pump pulse, and a scanning slit was introduced in the path of the terahertz pulse to provide the spatially dependent information.

The similarity between the generated pulses and the ideal TLPs was quantified by following the tomography approach of ref. [27] (Supplementary Section 10 presents details).

Data availability

The data from this paper can be obtained from the University of Southampton ePrints research repository at https://doi.org/10.5258/SOTON/D2261.

Reference

50. Lozovoy, V. V., Pastirk, I. & Dantus, M. Multiphoton intrapulse interference. IV. Ultrashort laser pulse spectral phase characterization and compensation. *Opt. Lett.* **29**, 775–777 (2004).

Acknowledgements

We are grateful to S. Pidishety for experimental assistance. This work was supported by the UK Engineering and Physical Sciences Research Council (grant no. EP/ M009122/1), MOE Singapore (grant no. MOE2016-T3- 1-006), the European Research Council (Advanced grant FLEET-786851, funder ID https://doi.org/10.13039/501100000781) and the Defense Advanced Research Projects Agency (DARPA) under the Nascent Light Matter Interactions programme. T.E. acknowledges funding for this research from the European Research Council under the European Union's Horizon 2020 research and innovation programme (grant agreement no. 715362). G.L. and T.E. acknowledge support from an NSFC-ISF joint grant (grant no. 12161141010; 3450/21). G.L. is financially supported by the National Natural Science Foundation of China (91950114 and 11774145), Guangdong Provincial Innovation and Entrepreneurship Project (2017ZT07C071) and the Natural Science Foundation of Shenzhen Innovation Commission (grant no. JCYJ20200109140808088).

Author contributions

A.Z. performed the optical experiments with support from N.P. and N.I.Z. Y.S. performed experiments to verify the absence of OAM in TLPs. C.M. performed the terahertz experiments with support from T.E. J.D. fabricated the terahertz meta-surface. T.E. and G.L. supervised the terahertz part. All authors contributed to the analysis and interpretation of the results. N.P. and N.I.Z. wrote the manuscript with input from all authors. N.I.Z. supervised the work.

Competing interests

The authors declare no competing interests.

Additional information

Supplementary information The online version contains supplementary material available at https://doi.org/10.1038/s41566-022-01028-5.

Correspondence and requests for materials should be addressed to Nikitas Papasimakis.

Peer review information *Nature Photonics* thanks Shuang Zhang and the other, anonymous, reviewer(s) for their contribution to the peer review of this work.

Reprints and permissions information is available at www.nature.com/reprints.